A Section 508–conformant HTML version of this article is available at https://doi.org/10.1289/EHP5701.

Effects of Aluminum on the Integrity of the Intestinal Epithelium: An *in Vitro* and *in Vivo* Study

Chang Hee Jeong,[1] Hyuk Cheol Kwon,[1] Do Hyun Kim,[1] Wei Nee Cheng,[1] Sukyung Kang,[2] Dong-Min Shin,[1] Jong Hyeok Yune,[1] Jee Eun Yoon,[1] You Hyun Chang,[1] Hyejin Sohn,[1] and Sung Gu Han[1]

[1]Toxicology Laboratory, Department of Food Science and Biotechnology of Animal Resources, Konkuk University, Seoul, Republic of Korea
[2]Department of Internal Medicine, College of Medicine, Severance Biomedical Science Institute, Yonsei University, Seoul, Republic of Korea

Background: Aluminum (Al) is the most abundant and ubiquitous metal in the environment. The main route of human exposure to Al is through food and water intake. Although human exposure to Al is common, the influence of Al on the gastrointestinal tract remains poorly understood.

Objectives: We aimed to further understand the toxic effect of Al and to elucidate the underlying cellular mechanisms in the intestinal barrier.

Methods: The human intestinal epithelial cell line HT-29 and C57BL6 mice were exposed to $AlCl_3$ at 0–16 mM (1–24 h) and 5–50 mg/kg body weight (13 weeks), respectively. In cell culture experiments, intracellular oxidative stress, inflammatory protein and gene expression, and intestinal epithelial permeability were measured. In animal studies, histological examination, gene expression, and myeloperoxidase (MPO) activity assays were conducted.

Results: Cellular oxidative stress level (superoxide production) in $AlCl_3$-treated cells (4 mM, 3 h) was approximately 38-fold higher than that of the control. Both protein and mRNA expression of tight junction (TJ) components (occludin and claudin-1) in $AlCl_3$-treated cells (1–4 mM, 24 h) was significantly lower than that of the control. Transepithelial electrical resistance (TEER) decreased up to 67% in $AlCl_3$-treated cells (2 mM, 24 h) compared with that of the control, which decreased approximately 7%. Al activated extracellular signal-regulated kinase 1/2 and nuclear factor-kappa B (NF-κB), resulting in mRNA expression of matrix metalloproteinase-9, myosin light-chain kinase, and inflammatory cytokines [tumor necrosis factor alpha (TNF-α), interleukin-1β (IL-1β), and IL-6] in HT-29 cells. Moreover, oral administration of $AlCl_3$ to mice induced pathological alteration, MPO activation, and inflammatory cytokine (TNF-α, IL-1β, and IL-6) production in the colon.

Conclusion: Al induced epithelial barrier dysfunction and inflammation via generation of oxidative stress, down-regulation of the TJ proteins, and production of inflammatory cytokines in HT-29 cells. In addition, Al induced toxicity in the colon by increasing the levels of inflammatory cytokines and MPO activity and induced histological damage in a mouse model. Our data suggest that Al may be a potential risk factor for human intestinal diseases. https://doi.org/10.1289/EHP5701

Introduction

Aluminum (Al) is the most abundant and ubiquitous metal element in the environment (Crisponi et al. 2012). Human exposure to Al is mostly through dietary intake and beverages. Aluminum compounds are widely used in food additives, antacids, pharmaceuticals, food packaging, and cooking utensils. In particular, Al salts (e.g., aluminum chloride, aluminum nitrate, aluminum sulfate) used in the water treatment process to reduce suspended particle, organic matter, and bacteria levels may increase Al concentrations in drinking water (Miller et al. 1984). The joint Food and Agriculture Organization of the United Nations (FAO)/World Health Organization (WHO) Expert Committee on Food Additives (JECFA) established the provisional tolerable weekly intake (PTWI) of 2 mg Al/kg body weight (BW) based on toxicological and bioavailability data (WHO/FAO 2011). Consumption levels of Al exceeding those recommended by the JECFA might be a risk factor for human health. For instance, excessive intake of Al can accumulate in tissues, and the bioaccumulation of Al can cause toxic responses in various tissues, including the brain, kidney, bone, and nervous system (Becaria et al. 2002). Several studies have shown that Al has been implicated in the progression of Alzheimer's disease (AD), possibly through the promotion of amyloid plaques (Bhattacharjee et al. 2014). Specifically, Praticò et al. (2002) showed that mice overexpressing the human amyloid precursor protein and fed dietary aluminum had more amyloid plaques than those who were not fed aluminum (Praticò et al. 2002). In addition, Yumoto et al. (2009) reported Al was detected in amyloid fiber in the senile plaques obtained from both the hippocampus and the temporal lobe in patients with AD (Yumoto et al. 2009). Furthermore, it was reported that male rats administered intraperitoneal Al three times per week for 3 weeks accumulated Al in the kidney, which is one of the main routes of elimination of Al from the body, exhibited signs of renal tubular cell deterioration and had higher lipid peroxidation, suggesting oxidative damage to cellular proteins and lipids (Mahieu et al. 2003).

The intestinal epithelium is in direct contact with different substances present in the diet and plays a crucial role as a barrier against the permeation of hazardous substances (Odenwald and Turner 2017). This intestinal barrier function relies on mucosal structural components (e.g., a hydrated gel composed of mucins) and intercellular junctions [e.g., tight junction (TJ), and adherens junction] (Kumar et al. 2018; Marchiando et al. 2010). The TJs are membrane domains with multi-protein complexes composed of integral transmembrane proteins and are important for determining paracellular permeability. The integral transmembrane proteins (i.e., occludins, claudins, and junctional adhesion molecules) regulate paracellular permeability by forming selectively permeable seals (Lee 2015). Thus, disruption of TJs and the subsequent increase in TJ permeability resulted in intestinal epithelial barrier dysfunction, limiting its functionality and potential consequences of intestinal diseases, including inflammatory bowel disease (IBD) and Crohn's disease (Schmitz et al. 1999; Schulzke et al. 2009). Furthermore, a higher expression of pro-inflammatory cytokines was frequently observed in 42 patients with IBD compared with 10 healthy controls (Singh et al. 2016). In particular, the pro-inflammatory cytokines tumor necrosis factor alpha (TNF-α; Ma et al. 2005) and interleukin 1 beta (IL-1β; Al-Sadi et al. 2008) increased TJ permeability via up-regulation of myosin light-chain

Address correspondence to Sung Gu Han, Animal Science Building #618, Konkuk University, 120 Neungdong-ro, Gwangjin-gu, Seoul 05029, Republic of Korea. Email: hansg@konkuk.ac.kr

Supplemental Material is available online (https://doi.org/10.1289/EHP5701).

The authors declare they have no actual or potential competing financial interests.

Received 2 June 2019; Revised 23 December 2019; Accepted 8 January 2020; Published 23 January 2020.

kinase (MLCK) expression, and IL-6 increased TJ permeability via activation of the c-jun N-terminal kinases (JNK) signaling pathway in Caco-2 cells (Al-Sadi et al. 2014).

Previous studies have reported that the oral bioavailability of Al was low, between 0.1% and 0.3% of ingested Al (Powell and Thompson 1993; Yokel et al. 2008). Given that the colon is the route of excretion of unabsorbed Al, it may be an important target for Al toxicity. However, Al toxicity in terms of homeostasis of intestinal mucosal barrier has rarely been studied. Therefore, the aim of our study was to investigate the toxic effect of Al and the underlying cellular mechanisms in the human colon epithelial cell line HT-29 and a mouse model.

Materials and Methods

Materials

Roswell Park Memorial Institute (RPMI)-1640 medium (LM011-01), fetal bovine serum (FBS; S001-07), and trypsin (LS015-01) were obtained from WELGENE Inc. Phosphate buffered saline (PBS; 17-517Q) was obtained from Lonza. ProLong® Gold antifade reagent (P36931) containing 4,6-diamidino-2-phenylindole (DAPI), and antibodies for claudin-1 (51-9000) and occludin (40-6100) were purchased from Invitrogen. Antibodies for phospho-extracellular signal-regulated kinases1/2 (p-ERK1/2) (9101) and ERK1/2 (9102) were purchased from Cell Signaling Technology. Antibodies for glyceraldehyde 3-phosphate dehydrogenase (GAPDH; sc-25778), p65 (sc-372), Lamin B (sc-6216), goat anti-rabbit IgG-HRP (sc-2030), donkey anti-goat IgG-HRP (sc-2020), and an ERK1/2 inhibitor [PD98059 (PD); sc-3532] were obtained from Santa Cruz Biotechnology, Inc. DyLight™-488-conjugated anti-IgG (A120-10872) was purchased from Bethyl Laboratories. Anhydrous aluminum chloride (563919; Al 20.24%, Cl 79.76%) an nuclear factor-kappa B (NF-κB) inhibitor [Bay11-7085 (Bay); B5681], and Pierce bicinchoninic acid (BCA) protein assay kit (23225) were purchased from Sigma-Aldrich. Nitrocellulose membrane (10600002) was obtained from (GE Healthcare Bio-Sciences).

Cell Cultures and Treatments

The human colorectal adenocarcinoma cell line HT-29 was obtained from the American Type Culture Collection (ATCC). In our study, cells from passages 4 to 10 were used in all experiments. The cells were maintained in RPMI 1640 medium supplemented with antibiotics and 10% FBS at 37°C in a humidified atmosphere containing 5% carbon dioxide (CO_2). The medium was changed every 2–3 d. The cells were digested using 0.05% trypsin/0.53 mM ethylenediaminetetraacetic acid (EDTA) solution when they reached approximately 80% confluency in 10-cm dishes. The cells were seeded on 10-cm dishes, 6-well plates, 24-well inserts, or 96-well plates according to each assay and then grown to approximately 80% confluency and synchronized for 15 h in medium containing 1% FBS. After synchronization, the cells were treated with aluminum chloride ($AlCl_3$; 1–16 mM) for 1–24 h. In the control group, the cells were treated with PBS. The concentration range was chosen according to previous studies (Pineton de Chambrun et al. 2014; Yu et al. 2016).

Cell Viability Assay

Cell viability was measured using the 3-(4,5-dimethylthiazol-2yl)-2,5-diphenyl-2H-tetrazolium bromide (MTT; Amresco; 0793) assay. The MTT assay was performed as described previously (Van Meerloo et al. 2011). Briefly, the cells were incubated in a 96-well plate with $AlCl_3$ (1, 2, 4, 8, and 16 mM) or PBS (control) for 24 h ($n = 4$ wells/group). The cells were then incubated for 3 h in medium containing 10 µL of MTT solution (5 mg/mL in PBS). After removing the medium, acidic isopropanol was added to dissolve the formazan crystal. The absorbance of the sample was measured at 570 and 630 nm using a spectrophotometer (BioTek Instruments), and then the 630-nm optical density (OD) background value was subtracted from 570-nm OD value. Cell viability (percentage) was calculated as follows: (treated well OD)/(control well OD) × 100.

Measurement of Intestinal Epithelial Permeability

Transepithelial electrical resistance (TEER) was measured on HT-29 cells to determine the permeability of TJs using the Millicell ERS-2 Voltohmmeter (Millipore). The cells (3.2×10^4 cells/well) were seeded in a 24-well plate with polyethylene terephthalate hanging cell culture with 0.4-mm pores (Millipore; MCHT24H48). The growth medium was changed every 3 d. After 15 d, cell monolayers were pretreated with or without *N*-acetylcysteine (NAC; 5 mM, 1 h) or PD (20 µM, 1 h) ($n = 3$ wells/group). After these pretreatments, the initial TEER values were measured. Then, the cell monolayers were treated with $AlCl_3$ (2 mM) for up to 24 h, followed by the determination of TEER values at 6 h intervals. The TEER values at each time point were normalized to the initial value.

Determination of mRNA Level of Tight Junction Proteins, Pro-Inflammatory Cytokines, and Signaling Molecules by Real-Time Polymerase Chain Reaction

To analyze gene expression including the TJ proteins, pro-inflammatory cytokines, matrix metallopeptidase 9 (MMP-9), and MLCK, total RNA was extracted from the cells ($n = 3$ wells/group) and mouse colon sections ($n = 6$–8 colon sections/group) using TRIzol reagent (Ambion; 15596018). Reverse transcription was carried out using the TOPscript RT DryMIX kit (Enzynomics; RT200) according to the manufacturer's protocol. The level of mRNA expression was determined by real-time polymerase chain reaction (RT-PCR) using the Real-Time PCR System (Thermo Fisher Scientific) and 2X Real-Time PCR mix (SolGent; SRH81-M40h). The thermal cycling conditions were as follows: initially at 95°C for 15 min, followed by 40 cycles at 95°C for 20 s and 58°C for 40 s, and then at 60°C for 30 s. The expression of mRNA was relatively quantified using the ΔΔCq method with the level of GAPDH mRNA used as the housekeeping gene. Primers were obtained from BIONICS and designed as shown in Table 1.

Determination of the Expression of Tight Junction Proteins and Signaling Molecules by Western Blotting

To determine the effect of Al on the expression of TJ proteins and cellular signaling pathway, Western blotting was performed. HT-29 cells were grown until 80% confluency in a 6-well plate and then treated with $AlCl_3$ (0–4 mM; in PBS) for 1–24 h with or without pretreatment with NAC [5 mM; in deionized water (DW)], PD [20 µM; in dimethyl sulfoxide (DMSO)], or Bay (15 µM; in DMSO) for 1 h ($n = 3$ wells/group). The cells were treated with PBS, DW, or DMSO as a control. After treatments, the cells were washed with cold PBS and then lysed in radioimmunoprecipitation assay buffer containing 50 mM Tris (pH 8.0), 150 mM sodium chloride (NaCl), 1% Triton™ X-100, 0.5% sodium deoxycholate, 0.1% sodium dodecyl sulfate (SDS), and a protease inhibitor mixture (2 µg/mL aprotinin, 10 µg/mL leupeptin, 1 µg/mL pepstatin A, 1 mM phenylmethane sulfonyl fluoride (PMSF), 5 mM EDTA, 1 mM ethylene glycol-bis(2-aminoethylether)-*N,N,N′,N′*-tetraacetic acid (EGTA), 10 mM sodium fluoride, and 1 mM sodium orthovanadate). Cell lysates were collected by scraping and then were centrifuged at 4°C (18,000 × *g*, 15 min) to remove cell debris. The protein concentration in collected samples was determined using the BCA protein assay kit. Protein samples were separated by SDS-polyacrylamide get electrophoresis (SDS-PAGE) and

Table 1. Primers used for RT-PCR in this study.

Gene	Primer sequence 5′–3′
Occludin	(F) CTG AAG TGG TTC AGG AGC TTC CAT
(Human)	(R) CTT TGA CCT TCC TGC TCT TCC CTT
Claudin-1	(F) AAG ATG AGG ATG GCT GTC ATT GGG
(Human)	(R) CAT TGA CTG GGG TCA TAG GGT CAT
MMP-9	(F) CCT CGA ACT TTG ACA GCG ACA AGA
(Human)	(R) CTC CGG CAC TGA GGA ATG ATC TAA
MLCK	(F) CTC AGT GGC AGG AAA TCC TCA ACA
(Human)	(R) CAT GAG GCT TTT CCT CAG CAA CAG
TNF-α	(F) AAG CCC TGG TAT GAG CCC ATC TAT
(Human)	(R) AGG GCA ATG ATC CCA AAG TAG ACC
IL-1β	(F) TAC CTG AGC TCG CCA GTG AAA T
(Human)	(R) CCT GGA AGG AGC ACT TCA TCT GTT
IL-6	(F) ACA GCC ACT CAC CTC TTC AGA AC
(Human)	(R) TTT TCT GCC AGT GCC TCT TTG C
GAPDH	(F) GAC CCC TTC ATT GAC CTC AAC TAC
(Human)	(R) ATG ACA AGC TTC CCG TTC TCA G
TNF-α	(F) AGG GAT GAG AAG TTC CCA AAT GGC
(Mouse)	(R) GGC TAC AGG CTT GTC ACT CGA AT
IL-1β	(F) TTG ACG GAC CCC AAA AGA TGA AGG
(Mouse)	(R) ACA GCT TCT CCA CAG CCA CAA T
IL-6	(F) TTC TTG GGA CTG ATG CTG GTG A
(Mouse)	(R) TTA AGC CTC CGA CTT GTG AAG TGG
GAPDH	(F) AAC TCC CAC TCT TCC ACC TTC GAT
(Mouse)	(R) CCC TGT TGC TGT AGC CGT ATT CAT

Note: GAPDH, glyceraldehyde 3-phosphate dehydrogenase; IL, interleukin; MLCK, myosin light-chain kinase; MMP, metallopeptidase; RT-PCR, real-time polymerase chain reaction; TNF, tumor necrosis factor.

transferred onto nitrocellulose membranes. The membranes were blocked with 3% nonfat milk buffer for 1 h at room temperature (23–26°C) and then incubated overnight at 4°C with the primary antibodies. After washing, the membranes were incubated for 1.5 h with appropriate secondary antibody-conjugated horseradish peroxidase. The protein bands were visualized using enhanced chemiluminescence (ECL) detection reagent (Thermo Fisher Scientific; 32106) and quantified using ImageJ 1.x software (Schneider et al. 2012). GAPDH and Lamin B were used as internal or loading controls for TJ proteins and NF-κB, respectively. To compare p-ERK and total ERK, the same membrane was used after the stripping procedure as follows: the nitrocellulose membrane was placed in stripping buffer (1.875 mL of 1 M Tris-HCl (pH 6.7), 6 mL of 10% SDS, 0.210 mL of 14.2 M β-mercaptoethanol, and 21.915 mL of DW) for 30 min at 57°C with slight agitation. The membrane was washed three times for 5 min each with DW, followed by three times of tris-buffered saline with Tween 20® (TBST) washing for 10 min each. Next, the membrane was blocked and re-probed using the Western blotting procedure.

Evaluation of the Integrity of Tight Junction and Tight Junction Protein Expression by Immunofluorescence Microscopy

To evaluate the effect of Al on the expression of TJ proteins, immunofluorescence staining was conducted. The cells were grown in 24-well plates and treated with $AlCl_3$ (2 mM) for 24 h ($n = 3$ wells/group). The cells were fixed with 4% paraformaldehyde (PFA) for 15 min and permeabilized using PBS containing 0.1% Triton™ X-100 for 10 min. The cell monolayers were then blocked with a blocking buffer comprising 3% bovine serum albumin and 2% normal donkey serum for 1 h and then incubated with anti-occludin and anti-claudin-1 diluted in blocking buffer overnight at 4°C. After washing with PBS, the cells were incubated with DyLight™-488-conjugated anti-IgG for 1 h at room temperature (23–26°C). Next, the cells were washed with PBS followed by 4% PFA fixation. Images of cells were captured using a Nikon Eclipse Ts2R camera (Nikon).

Quantitative Assessment of Cellular Oxidative Stress

To determine Al-induced cellular reactive oxygen species (ROS) production, intracellular superoxide levels were measured using dihydroethidium (DHE; Invitrogen; D11347), staining as described previously (Han et al. 2013). HT-29 cells were grown until 80% confluency on a cover glass in 6-well plates and treated with $AlCl_3$ (1, 2, and 4 mM) or PBS (control) for 3 h ($n = 3$ wells/group). Next, the cells were incubated in medium containing 1 μM DHE for 30 min, and then washed twice with cold PBS to terminate staining. The cells were fixed with 4% PFA solution in PBS and incubated for 10 min. The cells were then mounted with ProLong® Gold antifade reagent containing DAPI to stain the nuclei. Superoxide produced by cells was determined using an Olympus IX71 fluorescence microscope, and the images were captured using an Olympus DP71 camera and DP controller software (version 2.2, DP2-BSW; Olympus Optical Co.). The DHE staining area (red fluorescence) was quantified using ImageJ software as described previously (National Institutes of Health) (Liu-Smith et al. 2016).

Nuclear Fractionation

To determine the level of NF-κB p65 translocation into the nuclei, nuclear fractionation was performed according to a previous study with some modifications (Scheinman and Avni 2009). The cells were grown in 10-cm plates and then treated with $AlCl_3$ (1, 2, and 4 mM) for 6 h ($n = 3$ wells/group). The cells were lysed with hypotonic buffer [20 mM Tris (pH 7.4), 10 mM NaCl, 3 mM magnesium chloride ($MgCl_2$), 0.5 mM PMSF, and 1 mM sodium fluoride (NaF)]. After the addition of 10% Triton™-X 100, cell lysates were centrifuged at 4°C ($650 \times g$, 10 min), and the supernatants were collected as the cytosolic fractions. The remaining pellets were resuspended in cell extraction buffer [10 mM Tris (pH 7.4), 2 mM sodium orthovanadate (Na_3VO_4), 100 mM NaCl, 1% Triton™ X-100, 1 mM EDTA, 10% glycerol, 1 mM EGTA, 0.1% SDS, 0.5 mM PMSF, 1 mM NaF, and 20 mM tetrasodium pyrophosphate ($Na_4P_2O_7$)]. The homogenates were then centrifuged at 4°C ($14{,}000 \times g$, 20 min), and the supernatants were collected as the nuclear fractions.

Measurement of MMP Activity Using Gelatin Zymography

The activity of MMP was evaluated as described previously (Pushpakumar et al. 2013) with some modifications. The cells were starved with serum-free medium and treated with $AlCl_3$ (1, 2, and 4 mM) for 24 h ($n = 3$ wells/group). The conditioned medium was centrifuged at 4°C ($650 \times g$, 10 min) to collect the supernatant. The concentration of proteins in the supernatant was measured using the BCA protein assay kit, and the samples were analyzed using 8% SDS-PAGE gel containing 0.2% gelatin as MMP-9 substrate. After electrophoresis, the gel was washed with washing buffer containing 2.5% Triton™ X-100 to remove SDS. The gel was then incubated overnight at 37°C in a reaction buffer solution containing Tris-HCl (40 mM), calcium chloride ($CaCl_2$; 5 mM), and sodium azide (NaN_3; 3 mM). The MMP-9 activity was then determined by negative staining with Coomassie brilliant blue (Sigma-Aldrich; B-0630).

Animals and Treatments

Seven-week-old C57BL6 male mice (20–25 g) and feed (5L79) were purchased from Orient Bio. The mice were housed (4 mice/cage) with Beta Chip® bedding (Northeastern Products) for 1 week under controlled temperature and humidity (20–24°C and 40–70%) conditions with 12 h light–dark cycles. Standard commercial mouse feed and DW were provided *ad libitum*. All experiments with mice were approved by the institutional animal care and use committee (IACUC) at the Ethics Committee of Konkuk University (Seoul,

Republic of Korea; IACUC No. KU18165), and the mice were treated humanely. The mice were randomly grouped into control, $AlCl_3$ 5 mg/kg BW, $AlCl_3$ 25 mg/kg BW, and $AlCl_3$ 50 mg/kg BW ($n = 8$ mice/group). The minimum animal dose of $AlCl_3$ (5 mg/kg BW) was chosen based on human dietary intake levels (JECFA, PTWI: 2 mg/kg BW), which was converted using a body surface area (BSA) normalization method (Reagan-Shaw et al. 2008). Briefly, the minimum $AlCl_3$ dose (5 mg/kg BW) for mouse was calculated as follows: PTWI (mg/kg) = Mouse dose (mg/kg) × {[Mouse *Km* (3)]/[Human *Km* (37)]}. The *Km* factor is the body weight (in kilograms) divided by BSA (in meters squared).

Accordingly, the weekly intake dose for mice was equal to the PTWI in humans. To represent a high level of human exposure, $AlCl_3$ concentrations of 25 and 50 mg/kg BW were used based on previous studies (Martinez et al. 2018; Sood et al. 2011). $AlCl_3$ was diluted in DW and administered to mice via gavage for 13 weeks (5 d/week). Fresh $AlCl_3$ solutions adjusted to mouse weight were prepared weekly. Two days after the last administration of $AlCl_3$, the mice were anesthetized by intraperitoneal injection of 2.5% tribromoethanol (Avertin; (Sigma; T48404) 0.5 mL/25 g), and the mouse colon was collected. The entire colon was removed and the colon length was measured. After the colon samples were rinsed with cold PBS to remove intestinal content, the colon weight was measured. Then, the colon weight and length were expressed as colon weight/length ratio (in grams per centimeter).

The colon tissues were then cut in three parts horizontally. The top and middle parts were preserved at −80°C for RT-PCR analysis and myeloperoxidase (MPO) activity assay, respectively. The bottom part was fixed in 10% formalin for histological examination.

Myeloperoxidase Activity Measurement

The colon tissue samples were homogenized in four volumes of MPO assay buffer (BioVision; K744-100) and centrifuged at 13,000 × *g* for 10 min at 4°C to remove insoluble material. The enzyme activity was then determined using a colorimetric assay kit (BioVision; K744-100) according to the manufacturer's instructions. The OD of the sample was measured at 450 nm using a spectrophotometer (BioTek Instruments).

Histological Examination

The colon tissue samples were fixed in 10% formalin overnight and embedded in paraffin. The paraffin sections were cut to 3.5 μm and de-waxed using xylene for histochemical staining. The sections were then stained with hematoxylin and eosin (H&E) and photographed using the Nikon Eclipse Ts2R camera (Nikon). Images of the stained tissues were evaluated by three independent investigators who were blinded to treatment information (C.H.J., S.K., and S.G.H.). Histological alteration was examined for inflammatory cell infiltration, epithelial changes, and mucosal architecture as main categories, as described previously (Erben et al. 2014). The inflammatory cell infiltration was evaluated for the following criteria: *a*) distribution in the lamina propria, *b*) the focal mucosal localization, and *c*) extension to subjacent layers such as the muscularis mucosa and submucosa. The following criteria were used for determination of epithelial changes: *a*) crypt abscesses, *b*) crypt hyperplasia, and *c*) loss of goblet cells, whereas the examination of mucosal architecture included the followed criteria: *a*) irregular crypts, *b*) crypt loss, and *c*) villous blunting.

Statistical Analysis

Data are presented as mean ± standard error of the mean (SEM). Statistical significance was determined using the one-way analysis of variance, independent two-sample *t*-test, and Tukey post hoc test. The tests were carried out using SPSS–PASW statistics software for Windows (version 18.0; SPSS). A $p < 0.05$ was considered to indicate statistically significant differences.

Results

Cell Viability of Al-Exposed Colorectal Epithelial Cells

$AlCl_3$ at concentrations of up to 4 mM did not influence cell viability compared with that of the control (PBS) in the MTT assay (Figure 1). The cells treated with $AlCl_3$ at higher concentrations (8–16 mM) showed a significantly lower cell viability than the control cells. Therefore, $AlCl_3$ concentrations of 1, 2, and 4 mM were selected for the subsequent analysis.

Effects of Al on Epithelial Barrier Integrity of Cells

TEER was measured in HT-29 cells to evaluate whether Al disrupted the monolayer integrity of cells. In cells treated with 2 mM $AlCl_3$, the TEER values were lower by approximately 30% after 24 h, compared with that in the control (Figure 2A). However, pretreatment of cells with NAC (5 mM, 1 h) or PD (20 μM, 1 h) recovered the TEER values (Figure 2A). In addition, $AlCl_3$ (1–4 mM) significantly decreased the protein and mRNA levels of TJ components (occludin and claudin-1) in cells in a concentration-dependent manner (Figure 2B,C). Furthermore, the fluorescence microscopy images showed that the TJ proteins, such as occludin and claudin-1, were degraded and diffused in cells treated with $AlCl_3$ (2 mM, 24 h), compared with those in the control (Figure 2D).

Al-Induced Oxidative Stress in Cells

The treatment of cells with $AlCl_3$ increased cellular superoxide generation in a concentration-dependent manner (Figure 3). $AlCl_3$-treated cells produced a 38-fold higher level of intracellular ROS ($AlCl_3$ 4 mM) than that of the control cells (Figure 3B).

Al-Induced Signaling Pathways in Cells

$AlCl_3$-treated cells had higher levels of ERK phosphorylation and NF-κB nuclear expression than the control cells (Figure 4A,B). However, NAC (5 mM, 1 h) and $AlCl_3$ (2 mM, 1 h)-treated cells had significantly lower levels of ERK phosphorylation than 2 mM

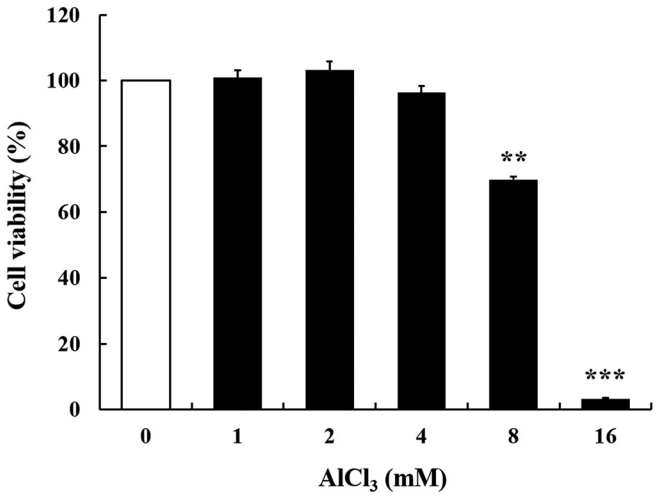

Figure 1. Effects of $AlCl_3$ on the viability of HT-29 cells. The MTT assay was performed to determine the viability of cells. The cells were treated with different concentrations of $AlCl_3$ for 24 h ($n = 4$ wells/group). The values represent the mean ± SEM ($n = 4$); $^{**}p < 0.01$ and $^{***}p < 0.01$ indicates a significant difference vs. the control (PBS). Note: MTT, 3-(4,5-dimethylthiazol-2yl)-2,5-diphenyl-2H-tetrazolium bromide; PBS, phosphate buffered saline; SEM, standard error of the mean.

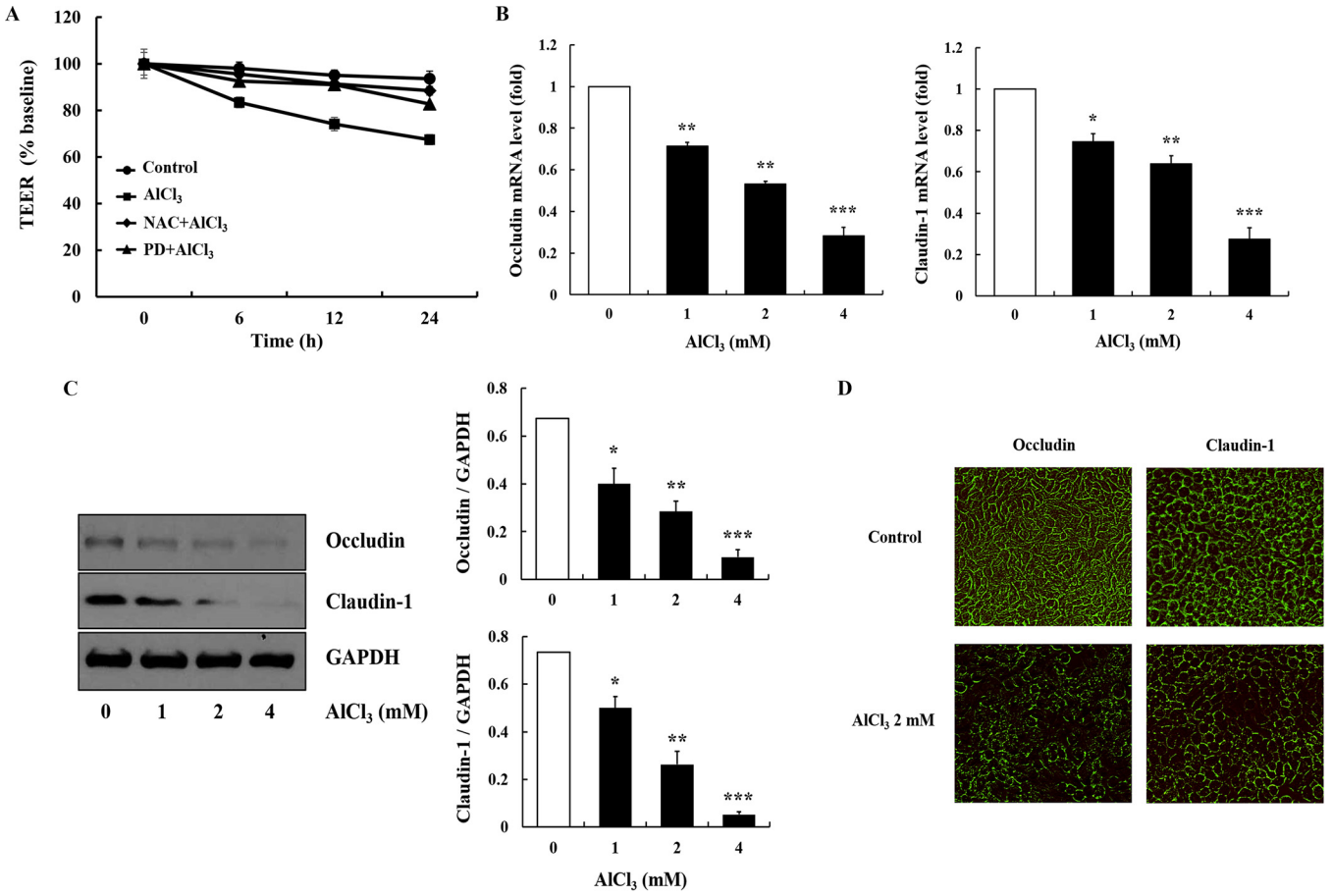

Figure 2. Measures informative of epithelial barrier function in HT-29 cells treated with $AlCl_3$. (A) Cell monolayers were treated with $AlCl_3$ (2 mM, up to 24 h) with or without pretreatment with *N*-acetylcysteine (NAC) (5 mM, 1 h) or PD98059 (PD) (20 μM, 1 h). Transepithelial electrical resistance (TEER) was measured in the cells ($n = 3$ wells/group). (B and C) Gene and protein expression of tight junction molecules. The cells were treated with $AlCl_3$ (0–4 mM, 12–24 h). The mRNA level (12 h) and protein expression (24 h) of occludin and claudin-1 were measured ($n = 3$ wells/group). Glyceraldehyde 3-phosphate dehydrogenase (GAPDH) was used as the housekeeping gene. (D) Fluorescence microscopy of occludin and claudin-1. The cells were treated with $AlCl_3$ (2 mM, 24 h). The images shown are representatives of three independent experiments. The values represent the mean ± SEM ($n = 3$); $^{*}p < 0.05$, $^{**}p < 0.01$, and $^{***}p < 0.001$ indicate a significant difference vs. the control (PBS). Note: PBS, phosphate buffered saline; SEM, standard error of the mean.

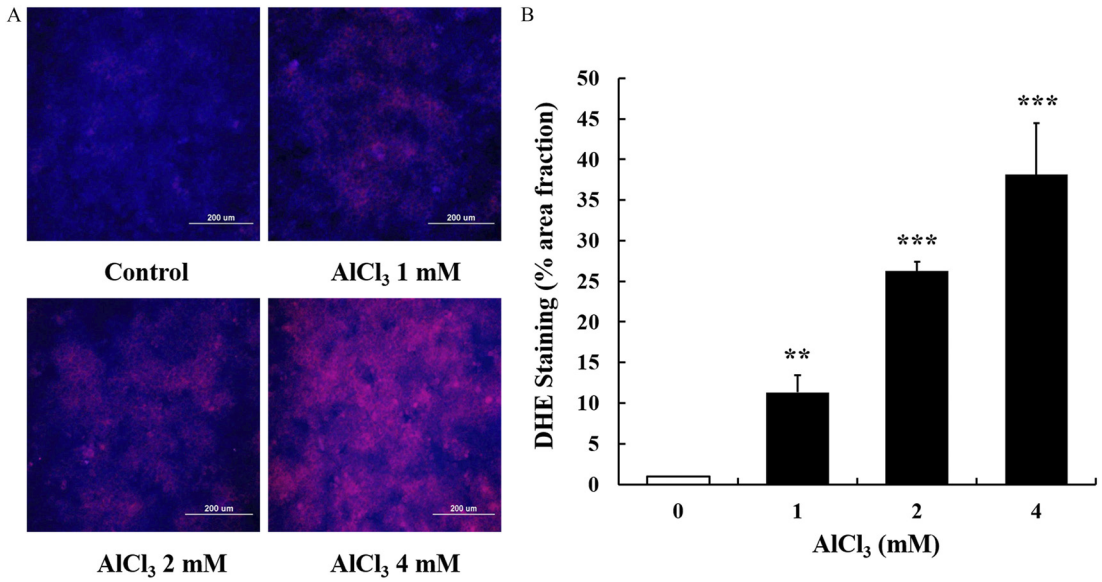

Figure 3. Dihydroethidium (DHE) staining for oxidative stress in HT-29 cells treated with $AlCl_3$. (A) Representative images showing the intensity of red fluorescence (intracellular production of superoxide anion). (B) Quantification of red fluorescent area. The images shown are representatives of three independent experiments. Scale bar: 200 μm. The values represent the mean ± SEM ($n = 3$); $^{**}p < 0.01$ and $^{***}p < 0.001$ indicate a significant difference vs. the control. Note: SEM, standard error of the mean.

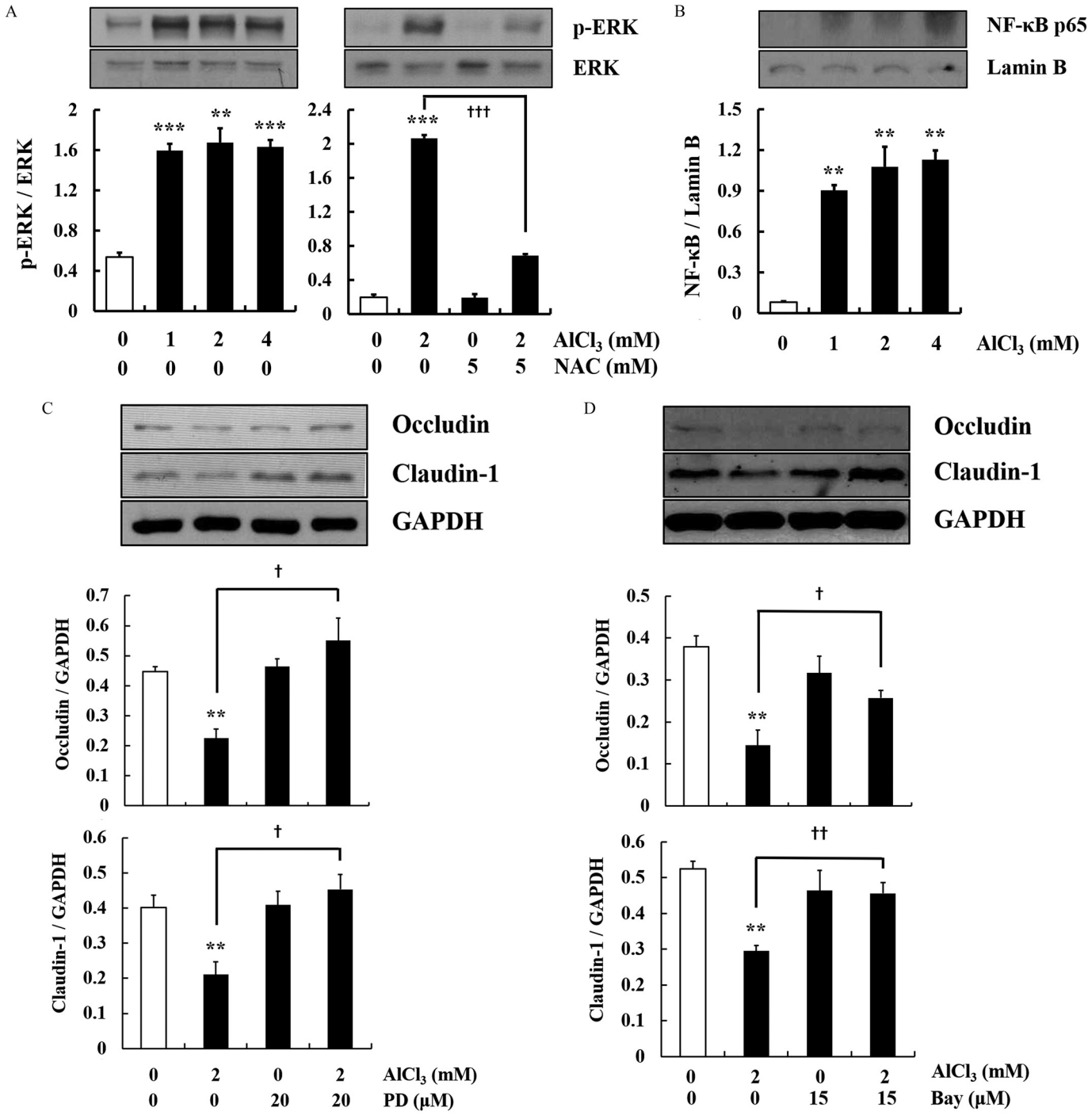

Figure 4. Markers of activation of the extracellular signal-regulated kinase 1/2 (ERK1/2) and nuclear factor-kappa B (NF-κB) pathways by $AlCl_3$ in HT-29 cells. (A) Phosphorylation of ERK in cells treated with $AlCl_3$ (0–4 mM, 1 h) with or without pretreatment with *N*-acetylcysteine (NAC; 5 mM, 1 h) ($n = 3$ wells/group). The level of p-ERK was compared with the level of total ERK by the stripping procedure. (B) Nuclear expression of NF-κB p65 in cells treated with $AlCl_3$ (0–4 mM, 6 h) ($n = 3$ wells/group). Lamin B was used as the nuclear housekeeping gene. (C and D) Cells were treated with $AlCl_3$ (2 mM, 24 h) with or without pretreatment with PD98059 (PD) (20 μM, 1 h) or Bay (15 μM, 1 h) ($n = 3$ wells/group). Glyceraldehyde 3-phosphate dehydrogenase (GAPDH) was used as the housekeeping gene. The Western blots shown are representative images of three independent experiments. The values represent the mean ± SEM ($n = 3$). $^{**}p < 0.01$ and $^{***}p < 0.001$ indicates a significant difference vs. the control (PBS); $^{\dagger}p < 0.05$, $^{\dagger\dagger}p < 0.01$, and $^{\dagger\dagger\dagger}p < 0.001$ indicates a significant difference vs. $AlCl_3$ alone. Note: Bay, Bay11-7085; PBS, phosphate buffered saline; SEM, standard error of the mean.

$AlCl_3$-treated cells (Figure 4A). To further confirm the involvement of ERK and NF-κB in Al-induced down-regulation of the TJ proteins, the cells were pretreated with pharmacological inhibitors of ERK (PD98059) or NF-κB (Bay 11-7082). Treatment with these inhibitors recovered the protein expression of occludin and claudin-1 down-regulated by Al exposure (2 mM) (Figure 4C,D).

To observe the role of MMPs and MLCK in Al-induced dysfunction of the epithelial barrier, the activity of MMP-9 and the mRNA expression of MMP-9 and MLCK were measured using gelatin zymography and RT-quantitative PCR (RT-qPCR). The treatment of cells with $AlCl_3$ increased the activity of MMP-9 (Figure 5A) and mRNA expression of MMP-9 and MLCK in a

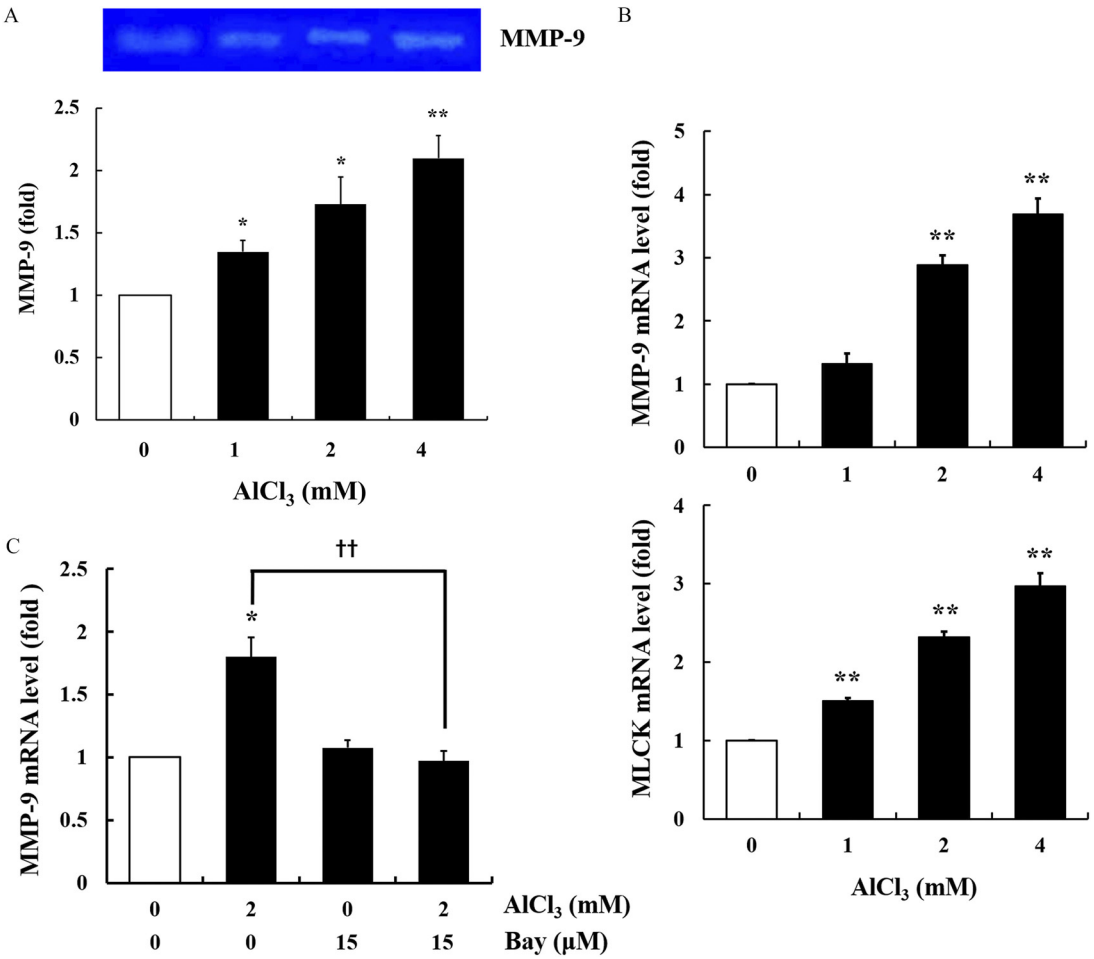

Figure 5. Activity of metalloproteinase-9 (MMP-9), and mRNA expression of MMP-9 and myosin light-chain kinase (MLCK) in $AlCl_3$-treated HT-29 cells. (A) The cells were treated with $AlCl_3$ (0–4 mM, 24 h). The MMP-9 activity in cultured medium was measured by gelatin zymography. The image shown is representative of three independent experiments. (B) Gene expression of MMP-9 and MLCK in cells treated with $AlCl_3$ (0–4 mM, 12 h) ($n = 3$ wells/group). Glyceraldehyde 3-phosphate dehydrogenase (GAPDH) was used as the housekeeping gene. (C) Gene expression of MMP-9 in cells pretreated with Bay (15 μM, 1 h), followed by $AlCl_3$ treatment (2 mM, 12 h) ($n = 3$ wells/group). Glyceraldehyde 3-phosphate dehydrogenase (GAPDH) was used as the housekeeping gene. The values represent the mean ± SEM ($n = 3$); $^{*}p < 0.05$ and $^{**}p < 0.01$ indicates a significant difference vs. the control (PBS); $^{\dagger\dagger}p < 0.01$ indicates a significant difference vs. $AlCl_3$ alone. Note: Bay, Bay11-7085; MLCK, myosin light-chain kinase; MMP, metallopeptidase; PBS, phosphate buffered saline; SEM, standard error of the mean.

concentration-dependent manner (Figure 5B). Furthermore, to identify whether MMP-9 activation was controlled by NF-κB activation, the cells were pretreated with an NF-κB inhibitor (Bay). Inhibition of the NF-κB pathway reduced the Al-induced mRNA up-regulation of MMP-9 to the control level (Figure 5C).

Expression of Pro-Inflammatory Cytokines in Cells

In the present study, we measured the mRNA levels of inflammation-associated cytokines (TNF-α, IL-1β, and IL-6) by RT-qPCR. $AlCl_3$-treated cells had a significantly higher mRNA expression of these cytokines than the control cells (Figure 6).

Colonic Inflammation in Mice

To provide further evidence of Al toxicity in the intestinal epithelium, an animal study was conducted using C57BL6 mice. The BW of mice treated with 25 and 50 mg/kg BW Al decreased by 5% and 1.5% after 2 weeks, respectively (Figure 7A). Thereafter, the BW of all mouse groups showed an increasing trend for 13 weeks (Figure 7A). Although the BW of all treatment groups increased, delayed weight gain was observed in a dose-dependent manner (Figure 7A). The mice administered higher levels of $AlCl_3$ (25 and 50 mg/kg BW) showed a lower BW gain despite no differences in feed intake (see Figure S1). Moreover, colonic MPO activity in $AlCl_3$-treated mice was significantly higher than that of the control (Figure 7B). The mice administered $AlCl_3$ presented a significantly increased colon weight/length ratio compared with that of the control (Figure 7C). In addition, the length of the mouse colon in $AlCl_3$-treated mice was shorter than that in the control (Figure 7D). Mouse colon samples were histologically examined by staining with H&E and observed using a microscope. $AlCl_3$ oral exposure induced crypt abscesses and hyperplasia, villous blunting, and inflammatory cell infiltration, which were not observed in the control (Figure 8A–C). Importantly, lower dose of $AlCl_3$ (5 mg/kg BW) also induced the aforementioned general indicators of intestinal inflammation. In addition, $AlCl_3$-treated mice had a significantly higher mRNA expression of inflammatory cytokines (TNF-α, IL-1β, and IL-6) in colon samples than that of the control mice (Figure 9).

Discussion

In the present study, the potential toxicity of Al was investigated in human colorectal epithelial cells and a mouse model. The results showed that Al exposure induced intestinal barrier dysfunction and

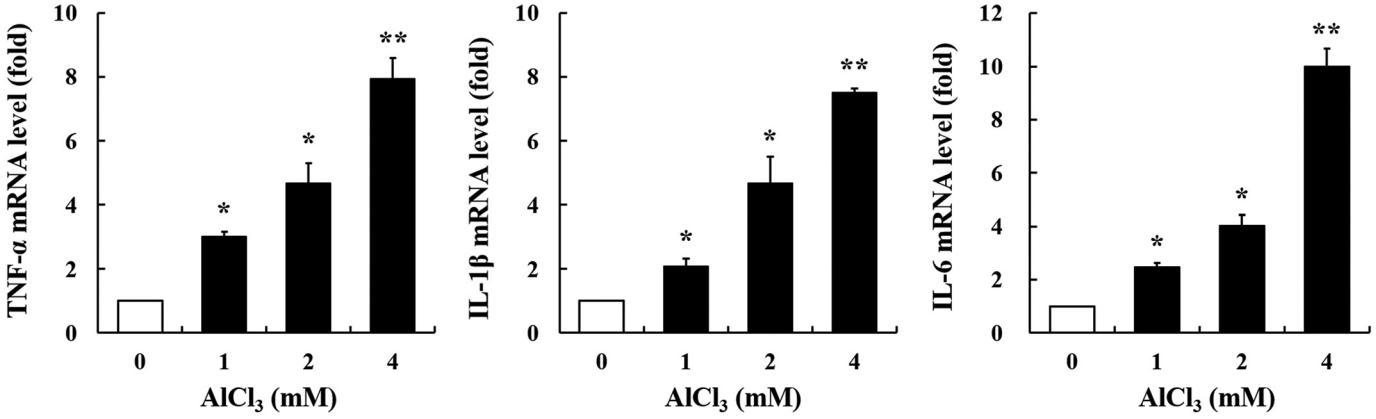

Figure 6. Gene expression of TNF-α, IL-1β, and IL-6 in $AlCl_3$-treated HT-29 cells. The cells were treated with $AlCl_3$ (0–4 mM, 12 h) ($n = 3$ wells/group). Glyceraldehyde 3-phosphate dehydrogenase (GAPDH) was used as the housekeeping gene. The values represent the mean ± SEM ($n = 3$); $^{*}p < 0.05$ and $^{**}p < 0.01$ indicate a significant difference vs. the control (PBS). Note: IL, interleukin; PBS, phosphate buffered saline; SEM, standard error of the mean; TNF, tumor necrosis factor.

inflammation via the accumulation of ROS that caused oxidative stress, down-regulation of the TJ proteins, and production of inflammatory cytokines in human colorectal epithelial cells. Our findings also demonstrated that Al induced the expression of inflammatory cytokines and histological alterations such as crypt abscesses, crypt hyperplasia, villous blunting, and inflammatory cell infiltration in the colon of mice.

In order to evaluate the effects of Al in the intestinal tract, we used two different experimental settings, a cell culture and a mouse model. We employed the human colorectal epithelial cell line HT-29 to evaluate Al toxicity at the cellular level. Furthermore, to determine the toxicity of Al in the intestinal barrier, C57BL6 mice were exposed to Al by gavage for 13 weeks.

We observed that Al at concentrations of up to 4 mM did not affect the viability of HT-29 cells. We first evaluated Al influence on the integrity of the intestinal epithelium by TEER analysis. $AlCl_3$-treated cells had a lower level of TEER than control cells, indicating that Al can disrupt intestinal barrier functions. $AlCl_3$ also significantly decreased the expression of the TJ proteins (occludin and claudin-1) in HT-29 cells. These TJ proteins are necessary for the formation of TJs that are essential for intestinal barrier functionality. The TJ is composed of multiple TJ protein complexes, forming

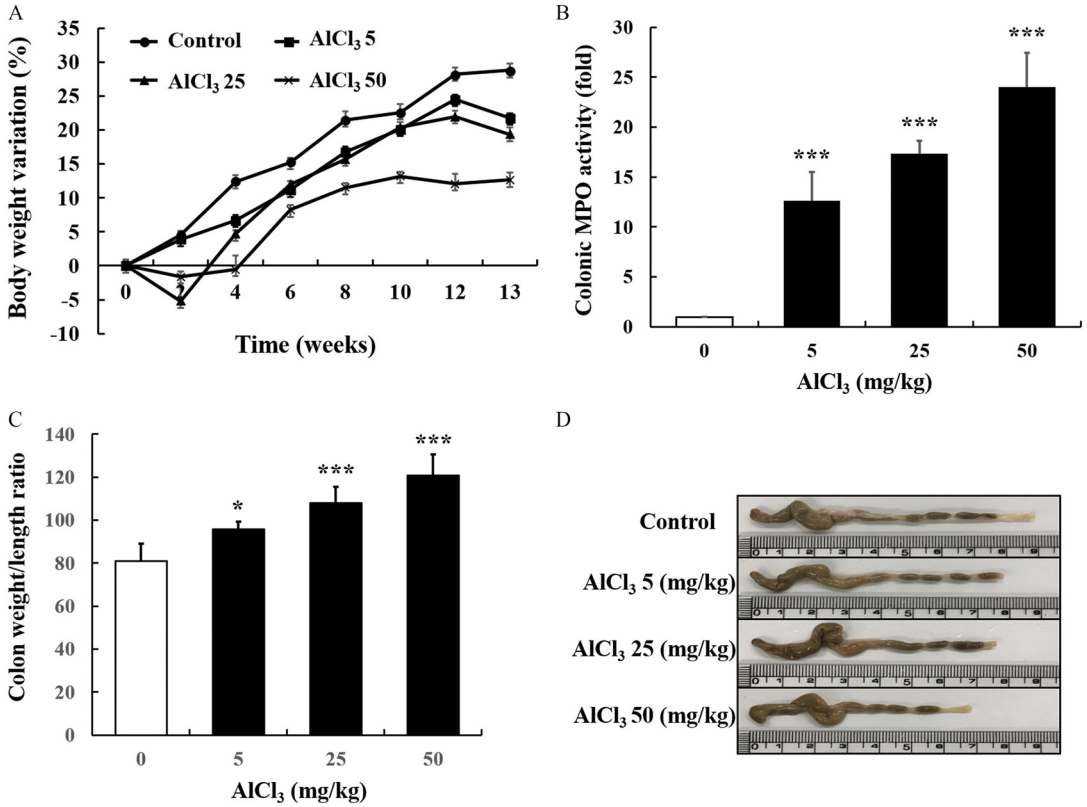

Figure 7. Effects of $AlCl_3$ in the colon of C57BL6 mice on (A) body weight variation, (B) MPO activity, and (C and D) colon weight and length of C57BL6 male mice after oral administration of $AlCl_3$ for 13 weeks. Mice received $AlCl_3$ at 5, 25, and 50 mg/kg body weight per day. The control group received deionized water (DW). The values represent the mean ± SEM (n = colon sections from 6–8 animals/group); $^{*}p < 0.05$ and $^{***}p < 0.001$ indicate significant differences vs. the control (DW). Note: MPO, myeloperoxidase; SEM, standard error of the mean.

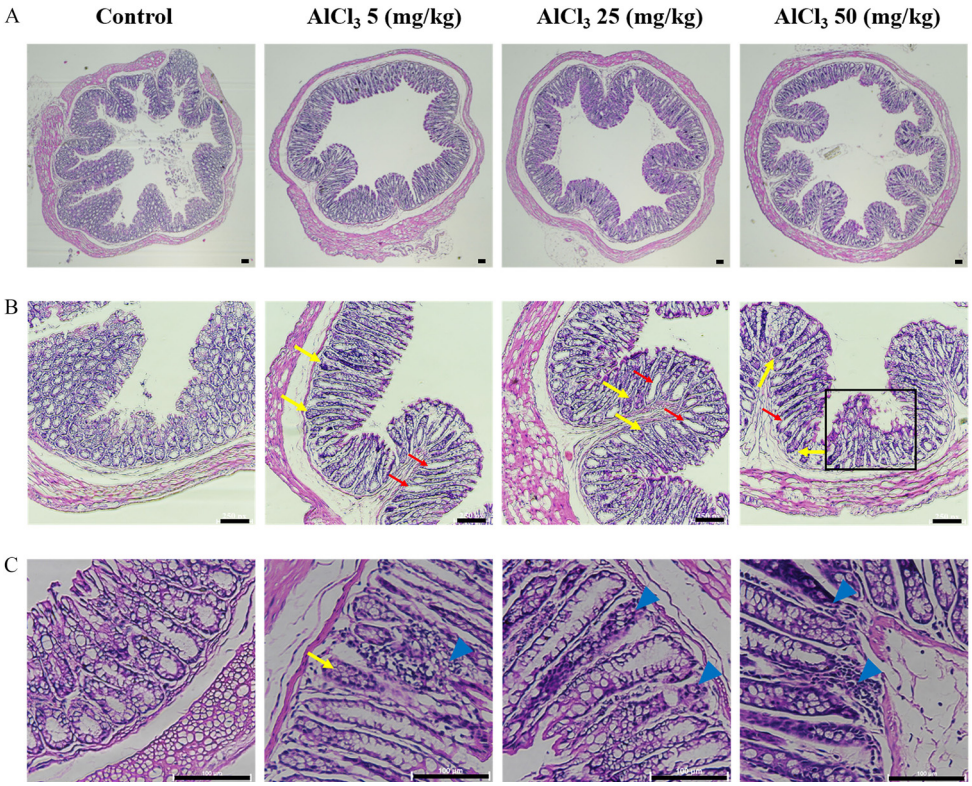

Figure 8. Histological data of $AlCl_3$-administered mouse colon. The data are representative images of hematoxylin and eosin (H&E)-stained mouse colon sections. (A) Whole images of a cross section (×40 magnification). (B) Abscesses (yellow arrows) and hyperplasia (red arrows) of the crypt and villous blunting (black box) (×150 magnification). (C) Abscesses of crypt (yellow arrows) and infiltration of inflammatory cells (blue arrowhead) (×400 magnification). Scale bar: 100 μm.

sealing strands embedded between both plasma membrane of adjacent cells. By regulating the density of the sealing strands, epithelial paracellular permeation can be controlled (Gumbiner and Louvard 1985; Simons and Fuller 1985). Hence, the TJ proteins play a critical role in preventing the permeation of hazardous substances, such as toxins and pathogens, into the intestinal epithelium (Lee 2015). Occludin, which was the first identified integral membrane protein in TJ structure, is particularly important for the regulation of intestinal epithelium permeability (Al-Sadi et al. 2011; Furuse et al. 1993). Along with occludin, claudin family proteins are key components of TJ structure, especially claudin-1, which can initiate TJ strand formation (Furuse et al. 1998; Landy et al. 2016). Therefore, down-regulation of these TJ proteins can disrupt the structural integrity of TJs, reducing their regulation of permeability, and thus, resulting in multiple intestinal diseases such as IBD (Edelblum and Turner 2009) and celiac disease (Khaleghi et al. 2016).

Next, we investigated the underlying cellular mechanisms of Al-induced TJ dysfunction. Previous studies in HT-29 cells (Jeong et al. 2017) and Caco-2 cells (N Wang et al. 2016) showed that oxidative stress was closely associated with a dysfunctional epithelial barrier. Our findings revealed that Al increased cellular ROS generation and disrupted intestinal epithelial integrity in HT-29 cells. Excessive oxidative stress in the gastrointestinal tract led to inhibition of the intracellular electron transport chain,

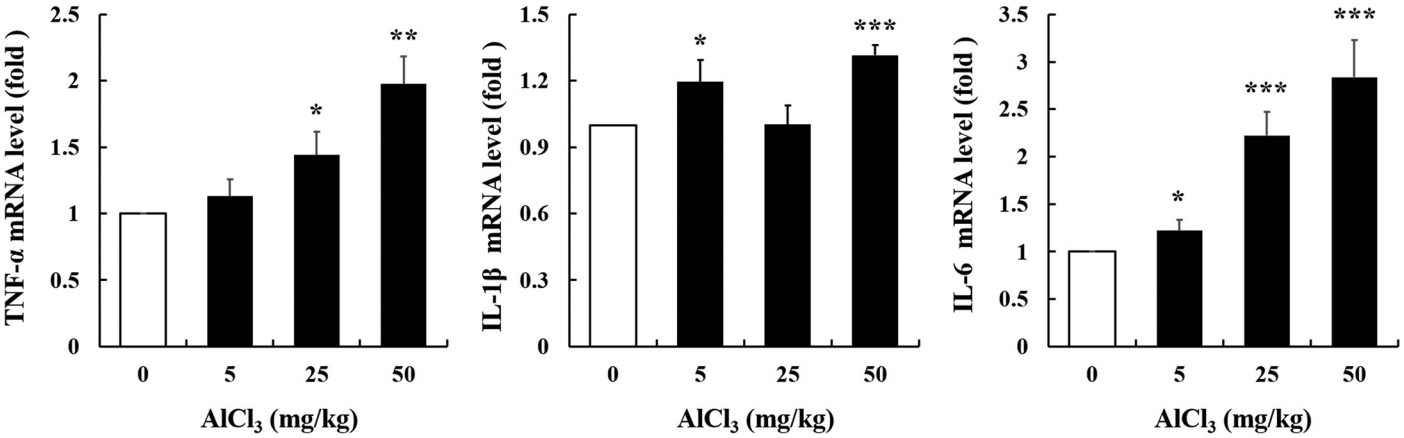

Figure 9. Gene expression of TNF-α, IL-1β, and IL-6 in $AlCl_3$-treated mouse colon tissue sample. Glyceraldehyde 3-phosphate dehydrogenase (GAPDH) was used as the housekeeping gene. The values represent the mean ± SEM ($n = 6–8$); $^{*}p < 0.05$, $^{**}p < 0.01$, and $^{***}p < 0.001$ indicate a significant difference vs. the control (DW). Note: DW, deionized water; IL, interleukin; TNF, tumor necrosis factor.

reduction in ATP production, and damage of DNA in the mitochondria of epithelial cells (Kowluru and Mishra 2015). This damage to the mitochondria resulted in intestinal epithelial dysfunction in mice (Berger et al. 2016). Moreover, Al-mediated ROS generation activated the ERK and NF-κB pathways in our study. These intracellular signaling molecules have been reported to be activated during disruption of junctional integrity (Berzal et al. 2015). Particularly, the increased activity of NF-κB may promote MMP-9 gene expression. To support this, Rangaswami et al. (2004) showed that there is an NF-κB binding site in the promoter region of the MMP gene in mouse melanoma cells (Rangaswami et al. 2004). According to a previous study, MMP-9 increased MLCK expression in C57BL/6 mice with dextran sulfate sodium (DSS)-induced intestinal inflammation (Nighot et al. 2015). In addition, in our study $AlCl_3$-treated cells had higher levels of MMP-9 and MLCK gene expression than control cells. A previous study using Caco-2 cells showed that increased MLCK plays a critical role in the dysfunction of the intestinal epithelial barrier by mediating perijunctional actomyosin interactions (Ma et al. 2000). In addition, in our study $AlCl_3$ significantly increased the production of inflammatory cytokines (TNF-α, IL-1β, and IL-6) in cells, which, in turn, can continually induce damage in intestinal epithelial cells via autocrine/paracrine action (Chen et al. 2015).

The dose of $AlCl_3$ (5 mg/kg BW) used in the animal experiments was selected based on the PTWI (2 mg/kg BW) established by the JECFA, which was translated from humans to animals using the BSA normalization method (Reagan-Shaw et al. 2008). This is because BSA accurately reflects some biological parameters in several mammalian species such as oxygen utilization rate, total blood volume, basal metabolism, calories burned, renal functions, and circulating plasma proteins (Reagan-Shaw et al. 2008). In a previous study, Al concentration (1.5 mg/kg BW) without BSA normalization did not directly induce an inflammatory response but, rather, exacerbated DSS-induced colitis in the mouse colon (Pineton de Chambrun et al. 2014). Thus, we hypothesized that $AlCl_3$ concentration (5 mg/kg BW) based on BSA normalization may more accurately portray the potential risks to human intestinal health. In addition, mice were administered with higher doses of $AlCl_3$ (25 and 50 mg/kg BW) to observe dose–response relationships. These mice showed a lower BW gain than control mice despite no differences in feed intake. It has been reported that mice administered DSS showed ulcerative colitis, which resulted in lower feed efficiency (Bitzer et al. 2016). Our data suggest that higher doses of Al induced inflammatory responses in the mouse colon such as ulcerative colitis, which resulted in lower feed efficiency and weight gain. In fact, our data confirmed that there are inflammatory responses such as the expression of pro-inflammatory cytokines in the mouse colon due to $AlCl_3$ exposure.

In mice administered $AlCl_3$, pathological changes were induced, including an increase in the colon weight/length ratio and MPO activity, up-regulation of inflammatory cytokines, and histological alteration in the mouse colon. Importantly, the lower dose of Al (5 mg/kg BW) also resulted in these inflammatory responses and pathological changes. Our data suggest that exposure of humans to Al within human dietary intake levels set by the JECFA can induce inflammatory and pathological responses in the intestinal epithelium after subchronic exposure. Indeed, these pathological characteristics have also been observed in human intestinal diseases such as IBD. Similar to our histological findings, patients with IBD have distorted crypt architecture, decreased crypt density, and increased inflammatory cells in crypt abscesses (Geboes 2001; Jenkins et al. 1997). However, in recent studies, chronic exposure to Al has been shown to be associated with different human diseases, including osteomalacia (Klein 2019) and AD (Z Wang et al. 2016). This indicates that Al might be associated with multiple human diseases. Further studies regarding Al exposure and the etiology of intestinal diseases are necessary.

Our data included both inflammatory responses of human colorectal cells in response to $AlCl_3$ exposure and the histopathological results in the mouse colon after subchronic oral administration of $AlCl_3$. Researchers have reported data about Al toxicity in the intestine. *In vitro* studies using HT-29 cells, Yu et al. (2016) found a lower expression of TJ proteins (e.g., ZO-1, occludin, claudin-1) and a higher level of oxidative stress when exposed to 4 mM Al ion than that of the control (Yu et al. 2016). Although their end points such as oxidative stress and TJ proteins are similar to those observed in our study, there was a lack of underlying mechanisms mediating Al toxicity within cells. In addition, Yu et al. (2016) selected only one high dose of Al ion (i.e., 4 mM), whereas our study provided a concentration–response relationship in the inflammatory process at concentrations of 1–4 mM $AlCl_3$. In another study using HT-29 cells, Djouina et al. (2016) focused on cell viability and the underlying mechanism (Djouina et al. 2016). They reported that 100–200 μg/mL (0.82–1.64 mM) $AlPO_4$ induced cell cycle arrest, apoptosis, and ROS generation. Some researchers have reported Al toxicity in the small intestine of rats. Bulan et al. (2015) showed that chronic exposure of aluminum sulfate induced degenerative tissue changes and oxidative parameters in the small intestine (Bulan et al. 2015). In this study, rats were injected intraperitoneally with 5 mg/kg aluminum sulfate [$Al_2(SO_4)_3$]. Because this is not a major route of Al exposure, their data from the small intestine samples provide only limited information. In another study, subchronic oral administration of $AlCl_3$ (50 mg/kg) to rats caused histopathological changes in the small intestine (Al-Qayim and Saadoon 2013). This study used H&E-stained sections without further biochemical analysis. In fact, these two studies focused more on the protective effects of melatonin and propolis against Al toxicity in the small intestine. They employed only a single dose of Al. Although further studies may be warranted using Al with different chemical forms, our study provided more robust and comprehensive data about the effects of Al in the intestine in comparison with these previous studies. Our data provided evidence about Al-induced cellular and molecular changes that led to epithelial barrier dysfunction and inflammatory responses in the colon, particularly administering a low dose of $AlCl_3$ to mice.

In conclusion, our results suggest that Al exposure can lead to a dysfunctional epithelial barrier and inflammatory response in colorectal epithelial cells by generating oxidative stress, activating ERK and NF-κB, increasing MMP and MLCK, and producing pro-inflammatory cytokines. Furthermore, the results of our animal study indicate that Al is a potential risk factor for inflammatory diseases in the colon.

Acknowledgments

This research was supported by the Basic Science Research Program through the National Research Foundation of Korea (NRF), funded by the Ministry of Education (2018R1D1A1B07046956).

References

Al-Qayim MAJ, Saadoon D. 2013. Assessment of the ameliorative role of proplis and malic acid in intestinal and liver functions of aluminum exposed male rats. Int J Sci Nat 4(3):552–558.

Al-Sadi R, Khatib K, Guo S, Ye D, Youssef M, Ma T. 2011. Occludin regulates macromolecule flux across the intestinal epithelial tight junction barrier. Am J Physiol Gastrointest Liver Physiol 300(6):G1054–G1064, PMID: 21415414, https://doi.org/10.1152/ajpgi.00055.2011.

Al-Sadi R, Ye D, Boivin M, Guo S, Hashimi M, Ereifej L, et al. 2014. Interleukin-6 modulation of intestinal epithelial tight junction permeability is mediated by JNK

pathway activation of claudin-2 gene. PLoS One 9(3):e85345, PMID: 24662742, https://doi.org/10.1371/journal.pone.0085345.
Al-Sadi R, Ye D, Dokladny K, Ma TY. 2008. Mechanism of IL-1β-induced increase in intestinal epithelial tight junction permeability. J Immunol 180(8):5653–5661, PMID: 18390750, https://doi.org/10.4049/jimmunol.180.8.5653.
Becaria A, Campbell A, Bondy S. 2002. Aluminum as a toxicant. Toxicol Ind Health 18(7):309–320, PMID: 15068131, https://doi.org/10.1191/0748233702th157oa.
Berger E, Rath E, Yuan D, Waldschmitt N, Khaloian S, Allgäuer M, et al. 2016. Mitochondrial function controls intestinal epithelial stemness and proliferation. Nat Commun 7:13171, PMID: 27786175, https://doi.org/10.1038/ncomms13171.
Berzal S, González-Guerrero C, Rayego-Mateos S, Ucero Á, Ocaña-Salceda C, Egido J, et al. 2015. TNF-related weak inducer of apoptosis (TWEAK) regulates junctional proteins in tubular epithelial cells via canonical NF-κB pathway and ERK activation. J Cell Physiol 230(7):1580–1593, PMID: 25536182, https://doi.org/10.1002/jcp.24905.
Bhattacharjee S, Zhao Y, Hill JM, Percy ME, Lukiw WJ. 2014. Aluminum and its potential contribution to Alzheimer's disease (AD). Front Aging Neurosci 6:62, PMID: 24782759, https://doi.org/10.3389/fnagi.2014.00062.
Bitzer ZT, Elias RJ, Vijay-Kumar M, Lambert JD. 2016. (-)-Epigallocatechin-3-gallate decreases colonic inflammation and permeability in a mouse model of colitis, but reduces macronutrient digestion and exacerbates weight loss. Mol Nutr Food Res 60(10):2267–2274, PMID: 27218415, https://doi.org/10.1002/mnfr.201501042.
Bulan NÖ, Sarikaya-Ünal G, Tunali S, Arda-Pirinççi P, Yanardağ R. 2015. Melatonin is a potent modulator of antioxidative defense and cellular proliferation against aluminum toxicity in rats. Turk J Biol 39:911–924, https://doi.org/10.3906/biy-1507-53.
Chen H, Min X-H, Wang Q-Y, Leung FW, Shi L, Zhou Y, et al. 2015. Pre-activation of mesenchymal stem cells with TNF-α, IL-1β and nitric oxide enhances its paracrine effects on radiation-induced intestinal injury. Sci Rep 5:8718, PMID: 25732721, https://doi.org/10.1038/srep08718.
Crisponi G, Nurchi VM, Bertolasi V, Remelli M, Faa G. 2012. Chelating agents for human diseases related to aluminium overload. Coord Chem Rev 256(1–2):89–104, https://doi.org/10.1016/j.ccr.2011.06.013.
Djouina M, Esquerre N, Desreumaux P, Vignal C, Body-Malapel M. 2016. Toxicological consequences of experimental exposure to aluminum in human intestinal epithelial cells. Food Chem Toxicol 91:108–116, PMID: 26995227, https://doi.org/10.1016/j.fct.2016.03.008.
Edelblum KL, Turner JR. 2009. The tight junction in inflammatory disease: communication breakdown. Curr Opin Pharmacol 9(6):715–720, PMID: 19632896, https://doi.org/10.1016/j.coph.2009.06.022.
Erben U, Loddenkemper C, Doerfel K, Spieckermann S, Haller D, Heimesaat MM, et al. 2014. A guide to histomorphological evaluation of intestinal inflammation in mouse models. Int J Clin Exp Pathol 7(8):4557–4576, PMID: 25197329.
Furuse M, Hirase T, Itoh M, Nagafuchi A, Yonemura S, Tsukita S, et al. 1993. Occludin: a novel integral membrane protein localizing at tight junctions. J Cell Biol 123(6 Pt 2):1777–1788, PMID: 8276896, https://doi.org/10.1083/jcb.123.6.1777.
Furuse M, Sasaki H, Fujimoto K, Tsukita S. 1998. A single gene product, claudin-1 or- 2, reconstitutes tight junction strands and recruits occludin in fibroblasts. J Cell Biol 143(2):391–401, PMID: 9786950, https://doi.org/10.1083/jcb.143.2.391.
Geboes K. 2001. Pathology of inflammatory bowel diseases (IBD): variability with time and treatment. Colorectal Dis 3(1):2–12, PMID: 12791013, https://doi.org/10.1111/j.1463-1318.2001.00187.x.
Gumbiner B, Louvard D. 1985. Localized barriers in the plasma membrane: a common way to form domains. Trends Biochem Sci 10(11):435–438, https://doi.org/10.1016/0968-0004(85)90026-X.
Han SG, Newsome B, Hennig B. 2013. Titanium dioxide nanoparticles increase inflammatory responses in vascular endothelial cells. Toxicology 306:1–8, PMID: 23380242, https://doi.org/10.1016/j.tox.2013.01.014.
Jenkins D, Balsitis M, Gallivan S, Dixon M, Gilmour H, Shepherd N, et al. 1997. Guidelines for the initial biopsy diagnosis of suspected chronic idiopathic inflammatory bowel disease. The British Society of Gastroenterology Initiative. J Clin Pathol 50(2):93–105, PMID: 9155688, https://doi.org/10.1136/jcp.50.2.93.
Jeong CH, Seok JS, Petriello MC, Han SG. 2017. Arsenic downregulates tight junction claudin proteins through p38 and NF-κB in intestinal epithelial cell line, HT-29. Toxicology 379:31–39, PMID: 28115242, https://doi.org/10.1016/j.tox.2017.01.011.
Khaleghi S, Ju JM, Lamba A, Murray JA. 2016. The potential utility of tight junction regulation in celiac disease: focus on larazotide acetate. Therap Adv Gastroenterol 9(1):37–49, PMID: 26770266, https://doi.org/10.1177/1756283X15616576.
Klein GL. 2019. Aluminum toxicity to bone: a multisystem effect? Osteoporos Sarcopenia 5(1):2–5, PMID: 31008371, https://doi.org/10.1016/j.afos.2019.01.001.
Kowluru RA, Mishra M. 2015. Oxidative stress, mitochondrial damage and diabetic retinopathy. Biochim Biophys Acta 1852(11):2474–2483, PMID: 26248057, https://doi.org/10.1016/j.bbadis.2015.08.001.
Kumar A, Chatterjee I, Anbazhagan AN, Jayawardena D, Priyamvada S, Alrefai WA, et al. 2018. *Cryptosporidium parvum* disrupts intestinal epithelial barrier function via altering expression of key tight junction and adherens junction proteins. Cell Microbiol 20(6):e12830, PMID: 29444370, https://doi.org/10.1111/cmi.12830.
Landy J, Ronde E, English N, Clark SK, Hart AL, Knight SC, et al. 2016. Tight junctions in inflammatory bowel diseases and inflammatory bowel disease associated colorectal cancer. World J Gastroenterol 22(11):3117–3126, PMID: 27003989, https://doi.org/10.3748/wjg.v22.i11.3117.
Lee SH. 2015. Intestinal permeability regulation by tight junction: implication on inflammatory bowel diseases. Intest Res 13(1):11–18, PMID: 25691839, https://doi.org/10.5217/ir.2015.13.1.11.
Liu-Smith F, Krasieva TB, Liu J, Liu J, Meyskens FL. 2016. Measuring redox status of melanoma cells. In: *Methods in Molecular Biology*. Totowa, NJ: Humana Press, 1–8, PMID: 27062599, https://doi.org/10.1007/7651_2016_352.
Ma TY, Boivin MA, Ye D, Pedram A, Said HM. 2005. Mechanism of TNF-α modulation of Caco-2 intestinal epithelial tight junction barrier: role of myosin light-chain kinase protein expression. Am J Physiol Gastrointest Liver Physiol 288(3):G422–G430, PMID: 15701621, https://doi.org/10.1152/ajpgi.00412.2004.
Ma TY, Hoa NT, Tran DD, Bui V, Pedram A, Mills S, et al. 2000. Cytochalasin B modulation of Caco-2 tight junction barrier: role of myosin light chain kinase. Am J Physiol Gastrointest Liver Physiol 279(5):G875–G885, PMID: 11052983, https://doi.org/10.1152/ajpgi.2000.279.5.G875.
Mahieu ST, Gionotti M, Millen N, Elías MM. 2003. Effect of chronic accumulation of aluminum on renal function, cortical renal oxidative stress and cortical renal organic anion transport in rats. Arch Toxicol 77(11):605–612, PMID: 12928767, https://doi.org/10.1007/s00204-003-0496-1.
Marchiando AM, Graham WV, Turner JR. 2010. Epithelial barriers in homeostasis and disease. Annu Rev Pathol 5(1):119–144, PMID: 20078218, https://doi.org/10.1146/annurev.pathol.4.110807.092135.
Martinez CS, Vera G, Ocio JAU, Peçanha FM, Vassallo DV, Miguel M, et al. 2018. Aluminum exposure for 60 days at an equivalent human dietary level promotes peripheral dysfunction in rats. J Inorg Biochem 181:169–176, PMID: 28865725, https://doi.org/10.1016/j.jinorgbio.2017.08.011.
Miller RG, Kopfler FC, Kelty KC, Stober JA, Ulmer NS. 1984. The occurrence of aluminum in drinking water. J Am Water Works Assoc 76(1):84–91, https://doi.org/10.1002/j.1551-8833.1984.tb05267.x.
Nighot P, Al-Sadi R, Rawat M, Guo S, Watterson DM, Ma T. 2015. Matrix metalloproteinase 9-induced increase in intestinal epithelial tight junction permeability contributes to the severity of experimental DSS colitis. Am J Physiol Gastrointest Liver Physiol 309(12):G988–G997, PMID: 26514773, https://doi.org/10.1152/ajpgi.00256.2015.
Odenwald MA, Turner JR. 2017. The intestinal epithelial barrier: a therapeutic target? Nat Rev Gastroenterol Hepatol 14(1):9–21, PMID: 27848962, https://doi.org/10.1038/nrgastro.2016.169.
Pineton de Chambrun G, Body-Malapel M, Frey-Wagner I, Djouina M, Deknuydt F, Atrott K, et al. 2014. Aluminum enhances inflammation and decreases mucosal healing in experimental colitis in mice. Mucosal Immunol 7(3):589–601, PMID: 24129165, https://doi.org/10.1038/mi.2013.78.
Powell JJ, Thompson RP. 1993. The chemistry of aluminium in the gastrointestinal lumen and its uptake and absorption. Proc Nutr Soc 52(1):241–253, PMID: 8493270, https://doi.org/10.1079/pns19930056.
Praticò D, Uryu K, Sung S, Tang S, Trojanowski JQ, Lee VM-Y. 2002. Aluminum modulates brain amyloidosis through oxidative stress in APP transgenic mice. FASEB J 16(9):1138–1140, PMID: 12039845, https://doi.org/10.1096/fj.02-0012fje.
Pushpakumar SB, Kundu S, Metreveli N, Tyagi SC, Sen U. 2013. Matrix metalloproteinase inhibition mitigates renovascular remodeling in salt-sensitive hypertension. Physiol Rep 1(3), PMID: 24159376, https://doi.org/10.1002/phy2.63.
Rangaswami H, Bulbule A, Kundu GC. 2004. Nuclear factor-inducing kinase plays a crucial role in osteopontin-induced MAPK/IκBα kinase-dependent nuclear factor κB-mediated promatrix metalloproteinase-9 activation. J Biol Chem 279(37):38921–38935, PMID: 15247285, https://doi.org/10.1074/jbc.M404674200.
Reagan-Shaw S, Nihal M, Ahmad N. 2008. Dose translation from animal to human studies revisited. FASEB J 22(3):659–661, PMID: 17942826, https://doi.org/10.1096/fj.07-9574LSF.
Scheinman EJ, Avni O. 2009. Transcriptional regulation of *Gata3* in T helper cells by the integrated activities of transcription factors downstream of the interleukin-4 receptor and T cell receptor. J Biol Chem 284(5):3037–3048, PMID: 19056736, https://doi.org/10.1074/jbc.M807302200.
Schmitz H, Barmeyer C, Fromm M, Runkel N, Foss H-D, Bentzel CJ, et al. 1999. Altered tight junction structure contributes to the impaired epithelial barrier function in ulcerative colitis. Gastroenterology 116(2):301–309, PMID: 9922310, https://doi.org/10.1016/S0016-5085(99)70126-5.
Schulzke JD, Ploeger S, Amasheh M, Fromm A, Zeissig S, Troeger H, et al. 2009. Epithelial tight junctions in intestinal inflammation. Ann NY Acad Sci 1165(1):294–300, PMID: 19538319, https://doi.org/10.1111/j.1749-6632.2009.04062.x.
Simons K, Fuller SD. 1985. Cell surface polarity in epithelia. Annu Rev Cell Biol 1:243–288, PMID: 3939606, https://doi.org/10.1146/annurev.cb.01.110185.001331.
Singh UP, Singh NP, Murphy EA, Price RL, Fayad R, Nagarkatti M, et al. 2016. Chemokine and cytokine levels in inflammatory bowel disease patients.

Cytokine 77:44–49, PMID: 26520877, https://doi.org/10.1016/j.cyto.2015.10.008.
Schneider CA, Rasband WS, Eliceiri KW. 2012. NIH Image to ImageJ: 25 years of image analysis. Nat Methods 9(7):671–675, PMID: 22930834, https://doi.org/10.1038/nmeth.2089.
Sood PK, Nahar U, Nehru B. 2011. Curcumin attenuates aluminum-induced oxidative stress and mitochondrial dysfunction in rat brain. Neurotox Res 20(4):351–361, PMID: 21656326, https://doi.org/10.1007/s12640-011-9249-8.
Van Meerloo J, Kaspers GJ, Cloos J. 2011. Cell sensitivity assays: the MTT assay. Methods Mol Biol 731:237–245, PMID: 21516412, https://doi.org/10.1007/978-1-61779-080-5_20.
Wang N, Han Q, Wang G, Ma W-P, Wang J, Wu W-X, et al. 2016. Resveratrol protects oxidative stress-induced intestinal epithelial barrier dysfunction by upregulating heme oxygenase-1 expression. Dig Dis Sci 61(9):2522–2534, PMID: 27146412, https://doi.org/10.1007/s10620-016-4184-4.
Wang Z, Wei X, Yang J, Suo J, Chen J, Liu X, et al. 2016. Chronic exposure to aluminum and risk of Alzheimer's disease: a meta-analysis. Neurosci Lett 610:200–206, PMID: 26592479, https://doi.org/10.1016/j.neulet.2015.11.014.
WHO/FAO (World Health Organization, Food and Agriculture Organization of the United Nations & Joint FAO/WHO Expert Committee on Food Additives). 2011. Evaluation of certain food additives and contaminants: seventy-fourth report of the Joint FAO/WHO Expert Committee on Food Additives. (WHO technical report series no. 966). https://apps.who.int/iris/bitstream/handle/10665/44788/WHO_TRS_966_eng.pdf?sequence=1&isAllowed=y [accessed 13 January 2020].
Yokel RA, Hicks CL, Florence RL. 2008. Aluminum bioavailability from basic sodium aluminum phosphate, an approved food additive emulsifying agent, incorporated in cheese. Food Chem Toxicol 46(6):2261–2266, PMID: 18436363, https://doi.org/10.1016/j.fct.2008.03.004.
Yu L, Zhai Q, Tian F, Liu X, Wang G, Zhao J, et al. 2016. Potential of *Lactobacillus plantarum* CCFM639 in protecting against aluminum toxicity mediated by intestinal barrier function and oxidative stress. Nutrients 8(12):783, PMID: 27918411, https://doi.org/10.3390/nu8120783.
Yumoto S, Kakimi S, Ohsaki A, Ishikawa A. 2009. Demonstration of aluminum in amyloid fibers in the cores of senile plaques in the brains of patients with Alzheimer's disease. J Inorg Biochem 103(11):1579–1584, PMID: 19744735, https://doi.org/10.1016/j.jinorgbio.2009.07.023.